Full Length Article

Directional local ternary quantized extrema pattern: A new descriptor for biomedical image indexing and retrieval

CrossMark

G. Deep [a,*], L. Kaur [b], S. Gupta [c]

[a] Department of CSE, IET Bhaddal, Punjab Technical University, Ropar, India
[b] Department of CE, Punjabi University (Pb.), Patiala, India
[c] Department of CSE, UIET, PU, Chandigarh, India

ARTICLE INFO

ABSTRACT

This paper proposes a new pattern descriptor called directional local ternary quantized extrema pattern (DLTerQEP) for biomedical image indexing and retrieval. The standard local binary patterns (LBPs) and local ternary patterns (LTPs) encode the gray scale relationship between the center pixel and its surrounding neighbors in two dimensional (2D) local region of an image whereas the proposed method encodes the spatial relation between any pair of neighbors in a local region along the given directions (i.e., 0°, 45°, 90° and 135°) for a given center pixel in an image. The novelty of the proposed method is it uses ternary patterns from horizontal–vertical–diagonal–antidiagonal ($HVDA_7$) structure of directional local extrema values of an image to encode more spatial structure information which lead to better retrieval. DLTerQEP also provides a significant increase in discriminative power by allowing larger local pattern neighborhoods. The experiments have been carried out for proving the worth of proposed algorithm on three different types of benchmark biomedical databases; (i) computed tomography (CT) scanned lung image databases named as LIDC-IDRI-CT and VIA/I-ELCAP-CT, (ii) brain magnetic resonance imaging (MRI) database named as OASIS-MRI. The results demonstrate the superiority of the proposed method in terms of average retrieval precision (ARP) and average retrieval rate (ARR) over state-of-the-art feature extraction techniques like LBP, LTP and LQEP etc.

1. Introduction

1.1. Motivation

Healthcare services today rely heavily on diverse biomedical imaging data which have been expanded exponentially in quantity – as there is rapid increase in the number of medical check-up per day; because of the use of diverse range of imaging modalities such as magnetic resonance imaging (MRI), ultrasound (US), computed tomography (CT), X-ray, etc. for different clinical studies. As we know that medical imaging is made up of dissimilar minor structures, there has been much interest of researchers in the development of well structured techniques to work on huge image databases of biomedical images for efficient access, search and retrieval. To sort out the problem of medical images, the knowledge of the content based image retrieval (CBIR) approach

is disseminated to develop content based medical image retrieval (CBMIR). Some comprehensive and extensive literature survey on CBIR systems is presented in Antani et al. [2], Jing and Allinson [21] and Yue et al. [69]. CBIR uses the visual content features such as color, texture, shape, and spatial layout etc. of regions or objects to represent and index the biomedical image database for efficient retrieval. These features are arranged as multi-dimensional feature vectors and stored in the feature database. The main step of the CBIR is feature extraction, the effectiveness of which rests upon the method derived for extracting features from given images. The selection of feature descriptors affects on image retrieval performance.

Nowadays, texture based features play an important role as powerful discriminating visual features. They are extensively used in the image processing applications to identify the visual patterns. Some of texture feature extraction methods are proposed by Haralick et al. [16], Tamura et al. [57] and Haralick [15]. WLD and BGP texture descriptors have proposed by Chen et al. [5] and Zhang et al. [72], respectively. Siqueira et al. [54] have proposed extended GLCM texture descriptors to multiple scales on benchmark texture data sets. Verma et al. [61] proposed local extrema co-occurrence

patterns (*LECoP*) in which *GLCM* is used to find a co-occurrence of the mapped pixels. Parida and Bhoi [50] used texture features to extract the objects from gray scale images. For the directional features based on texture retrieval, Do and Vetterli [6] have suggested the discrete wavelet transform (*DWT*) which extracts the features in three directions (horizontal, vertical and diagonal). Kokare et al. [27] have used rotated wavelet filters for image retrieval by collecting various image features in various directions. Kokare et al. [25], Kokare et al. [26] and Kokare et al. [27] advocated the amalgamation of the *DT-CWF*, *DT-RCWF* and also rotational invariant *DT-RCWF* to have some other directional features that are not present in *DWT*. Hussain and Triggs [18] have proposed the local quantized patterns (*LQP*) which collects the directional geometric features in horizontal, vertical, diagonal and anti-diagonal strips of pixels; combinations of horizontal–vertical, diagonal–antidiagonal and horizontal–vertical–diagonal–antidiagonal; and traditional circular and disk-shaped regions for visual recognition. Most of biomedical images represented in gray scale are extensively textured in common. Hence, in clinical exams, the appearance of organ/tissue/lesion in the images is due to intensity variations that laid on various texture characteristics. Thereafter, texture became very popular in biomedical image retrieval because of eminent significance of acquired texture. For example, Gibbs and Turnbull [11] got significant differences between benign and malignant lesions for a number of textural features on breast imaging. Felipe et al. [10] worked on retrieval of medical *CT* and *MRI* images in varied tissues using co-occurrence matrix. Traina et al. [59] proposed medical image retrieval system using wavelet transformations. Jhanwara et al. [20] have suggested content based image retrieval system using motif co-occurrence matrix (*MCM*) to delineate texture properties. Hajek et al. [14] have used the concept of texture analysis for magnetic resonance imaging and possible clinical application in that modality. Scott and Shyu [53] have utilized the concept of entropy balanced statistical (*EBS*) *k-d* tree on high-resolution computed tomography (*HRCT*) lung images for biomedical media retrieval system. Liu et al. [31] have described texture information using the technique of multi-scale complexity and multi-scale fractal dimension for medical image retrieval. Kassner and Thornhill [23] have shown texture analysis as valuable tool on neuro-*MR* imaging (brain tumors dataset). Ramamurthy et al. [51] explored intensity, texture features using fusion method from large scale of dental images. Nanni et al. [42] have proposed the texture descriptors by extending the *GLCM* to multi-scale based on Gaussian filtering and by extracting features which were tested on biomedical image classification problems, not only from the entire co-occurrence matrix but also from subwindows. Yadav et al. [67] have proposed a new approach with compressive sampling which extracts the texture features of large medical databases for retrieval. Vaidehi and Subashini [60] have proposed texture features for content-based mammogram retrieval. Irmak et al. [19] have worked on brain tumor images using medical image processing.

However, the computation complexity of the texture features calculated from *co-occurrence matrix* [10], *MCM* [20], *multi-scale fractal dimension* [31], *Multi-scale* texture descriptors [42], *compressive sampling* [67], etc., is more expensive. To address the same, the local binary pattern (*LBP*) by Ojala et al. [46] is proposed. *LBP* being having low computational complexity and capacity of coding minute specifications, Ojala et al. [47] advocated some more moderations in *LBP* for texture classifications. Takala et al. [56] proposed the block-based texture features using the *LBP* texture features for image retrieval. Heikkila et al. [17] used the combination of *LBP* features and scale invariant feature transform (*SIFT*) to introduce texture pattern method i.e., center symmetric local binary pattern (*CS-LBP*). *LBPs* have encoded using five discrete levels by Nanni et al. [43] and Nanni et al. [44]. Guo et al. [12] and Liu et al. [30] proposed the local configuration pattern (*LCP*) and binary
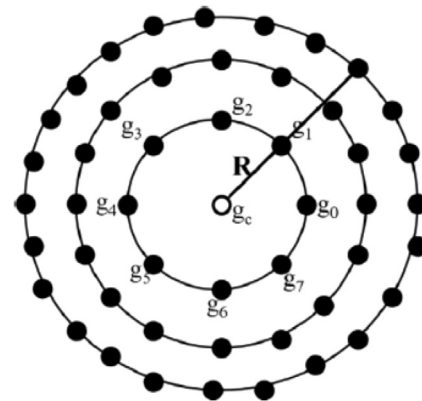

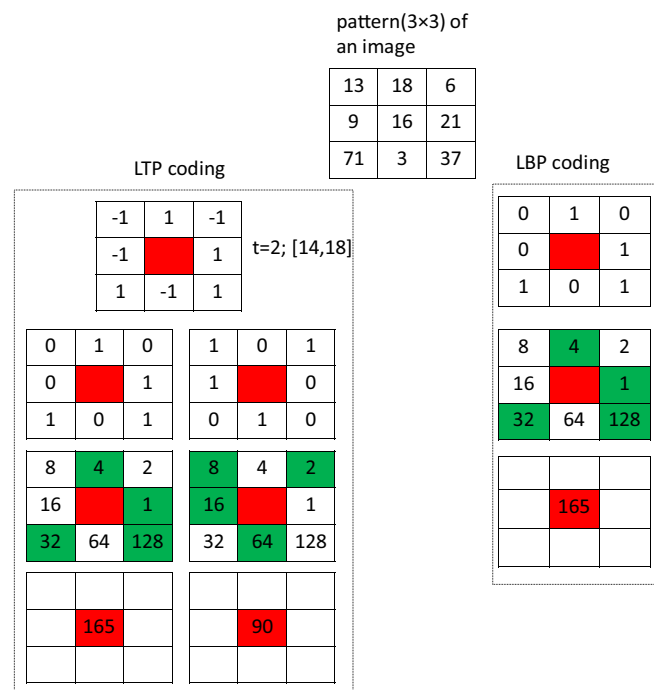**Fig. 1.** Circular neighborhood sets for different (*P*, *R*).

Fig. 2. Calculation of LBP and LTP operators.

rotation invariant and noise tolerant (*BRINT*) texture descriptors respectively using *LBPs*. Some of other *LBP* variants for texture image retrieval applications are proposed by Vipparthi and Nagar [65], Vipparthi and Nagar [66], Vipparthi et al. [64] and Bala and Kaur [3]. In the field of medicine, Oliver et al. [48] used *LBP* descriptor for mammogram images. Keramidas et al. [24] have given texture representation on thyroid ultrasound images. In (2008b, 2008c), Nanni and Lumini [40,41] used *LBP* to automate the cell phenotype image classification. In the area of face classification, Nanni and Lumini [38], Ahonen et al. [1] and Chen et al. [4] have extensively worked on *LBP*. Guo et al. [13] have proposed rotational invariant *LBP* variance operator for texture classification. Some important papers of Nanni and Lumini [39] and Zenghai et al. [70] have also successfully experimented *LBP* in other useful applications. More on *LBP* can be explored at http://www.ee.oulu.fi/mvg/page/lbp_bibliography#biomedical.

In the literature, Murala et al. [35], Murala et al. [36], Murala et al. [37], Murala and Jonathan [33], Murala and Jonathan [34], Dubey et al. [7], Dubey et al. [8], Dubey et al. [9] and Vipparthi et al. [63] have proposed many extended versions of *LBP* to obtain new image features for biomedical image indexing. As we know
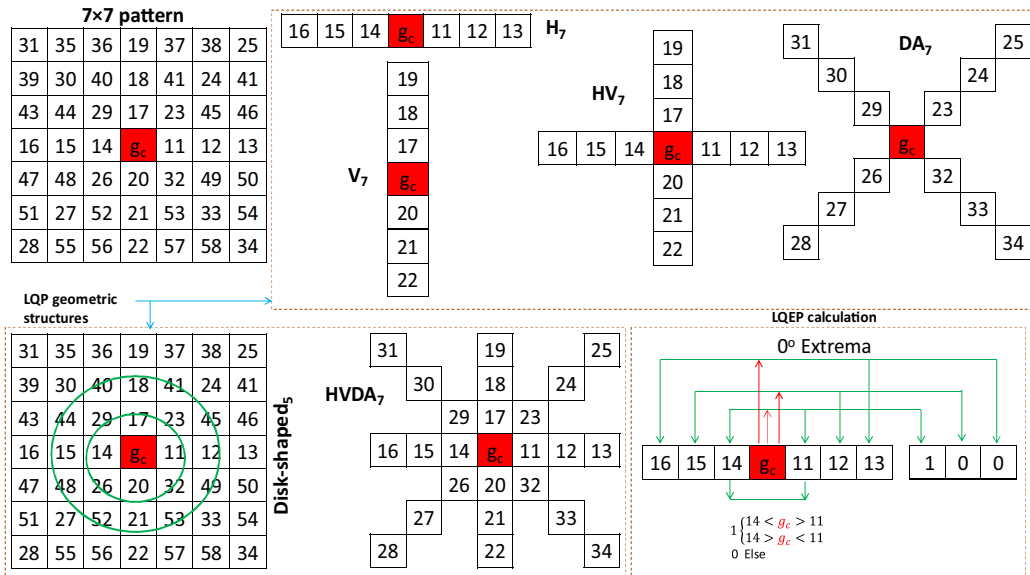
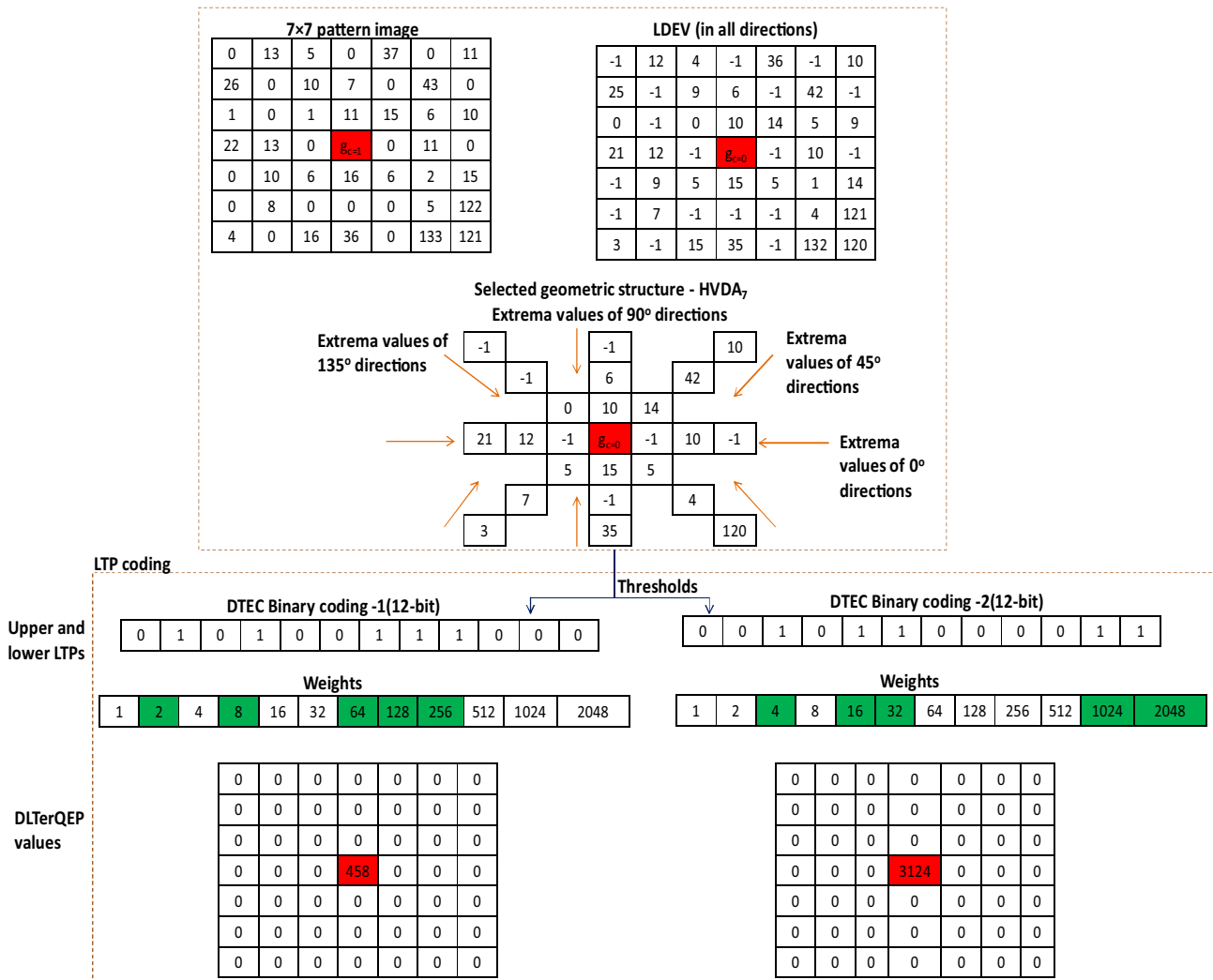**Fig. 3.** Example of LQEP feature calculation using HVDA$_7$ geometric structure for a given 7×7 pattern of an image.

Fig. 4. Example to obtain DLTerQEP calculation for 7×7 pattern of an Image.

Sample image

LBP feature map   LQEP feature map   DLTerQEP - upper LTP feature map   DLTerQEP - lower LTP feature map
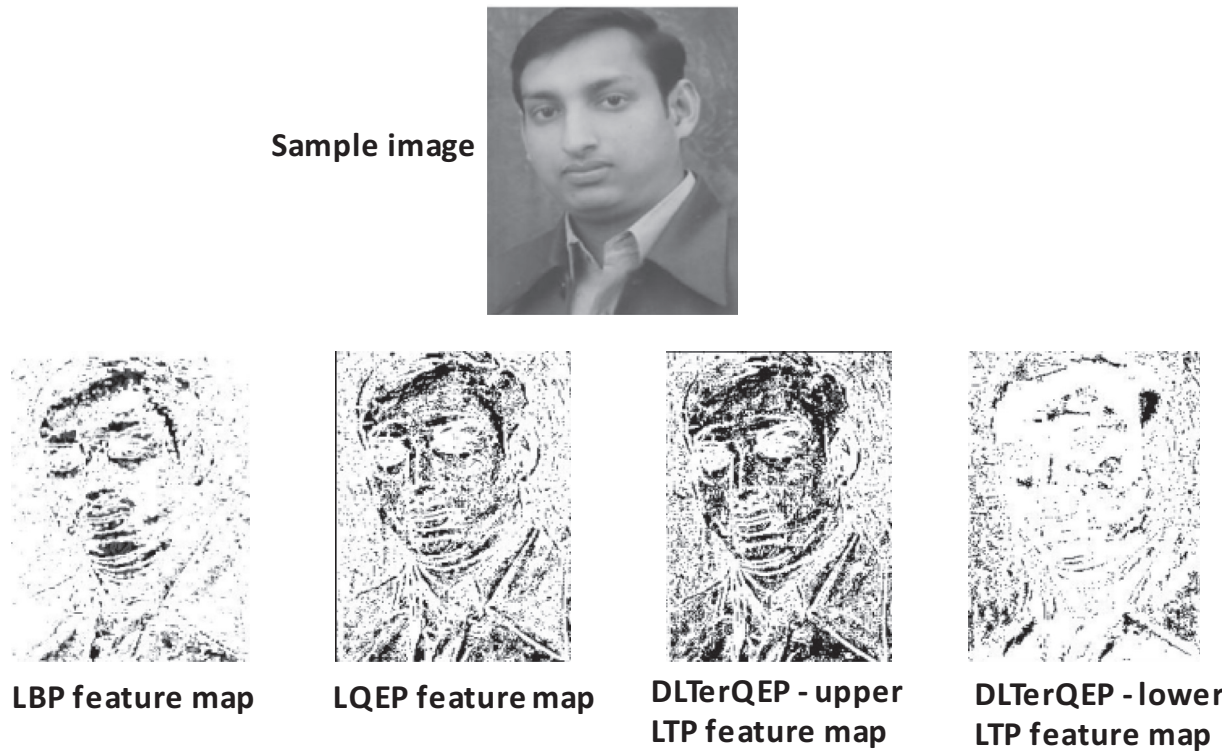
Fig. 5. Response of proposed method on a reference face.

that the *LBP* provides the first-order directional derivative patterns but Zhang et al. [71] examined *LBP* as non-directional first-order local patterns and have proposed local derivative patterns (*LDP*) for face recognition. Both *LBP* and *LDP* in the literature review cannot appropriately find out the appearance distinction of particular objects in natural images due to intensity variations. To handle this, Tan and Triggs [58] introduced local ternary pattern (*LTP*) for texture classification. *LTP* has small pixel value variations as compared to *LBP*. *LBP*, *LDP* and *LTP* capture the feature information based on the distribution of edges which are coded using only two directions (positive direction or negative direction). Paci et al. [49] have also presented in their research, the more discriminative features using non-binary coding on biological datasets than the binary one. In some more researches, Rao and Rao [52] have proposed local quantized extrema patterns (*LQEP*) for natural and texture image retrieval which encodes the spatial relation between any pair of neighbors in a local region along the given directions for a given center pixel in an image. To recognize the image, *LBP* features are calculated from directional quantized texture patterns in *LQEP*. The standard *LBP* method provides the connection between the referenced pixel and its neighbors in circumference. In contrast to *LBP*, *LQEP* method provides the connection between any pair of neighbors in a local region for a given referenced pixel in an image.

It has already been proved in Kokare et al. [25], Kokare et al. [26], Kokare et al. [27] and Hussain and Triggs [18] that the directional features are very significant in various applications of image retrieval. But, the most of above literature on *LBP* features and its improved versions gives non-directional features. After the research papers review above, in this paper, the local *2D* patterns; *LBP*, *LTP* and *LQEP* motivated us to propose the *DLTerQEP* for biomedical image indexing and retrieval. The main novelties of the proposed method (*DLTerQEP*) are as follows: (a) it is already proved by Tan and Triggs [58] that the *LBP* is sensitive to lighting variations, to address this problem, the concept of *LTP* is used. (b) It collects ternary patterns from horizontal–vertical–

diagonal–antidiagonal (*HVDA*$_7$) structure of directional local extrema values of an image to provide more spatial structure information which lead to better retrieval. (c) It also provides a significant increase in discriminative power by allowing larger local pattern neighborhoods. The performance of the proposed method is tested by conducting the experiments on three different types of benchmark biomedical databases.

The organization of the paper is as follows: in Section 1, a brief review of medical image retrieval and related work are given. A brief description of local patterns and proposed method can further be visualized in Section 2. Section 3 presents the concepts of proposed system framework and evaluation measures. Experimental results and discussions are presented in Section 4. Finally, the concluding remarks and future perspectives are given in Section 5.

2. Review of local patterns

2.1. Local binary patterns formulation (LBPs)

The *LBP* was first introduced by Ojala et al. [47] for rotation invariant texture classification. The *LBP* is very efficient texture descriptor due to its discriminative power and computational simplicity. Given an grayscale image *I* of size $n \times m$ pixels and *I(g)*denotes the gray level of the *g*th pixel in the image *I*. The *LBP* operator is calculated at each pixel by evaluating the binary differences of the values in a small circular neighborhood (with radius *R*) around the value of a central pixel, g_c. Mathematically, the *LBP* value of current pixel is given:

$$LBP_{P,R} = \sum_{p=0}^{P-1} f_1(g_p - g_c)2^p, f_1(x) = \begin{cases} 1, & \text{if } x \geqslant 0; \\ 0, & \text{otherwise}; \end{cases} \quad (1)$$

where g_c: gray value of the center pixel; g_p: gray values of the circularly symmetric neighborhood g_p ($p = 0, \ldots, P - 1$); *P*: image pixels

Sample image

7×7 pattern image

3×3 pattern image

LBP(8,1)

LBP pattern

LTP pattern

upper and lower
LTP histograms

Feature vector

LDEV

Local directional extrema values in possible directions

HVDA$_7$ geometric shape

Extrema values (in 0°, 45°, 90° and 135° directions)

DTEC LTP patterns

DTEC LTP coding
pattern -1

DTEC LTP coding
pattern -2

DLTerQEP patterns

DLTerQEP pattern
for upper LTP

DLTerQEP pattern
for lower LTP
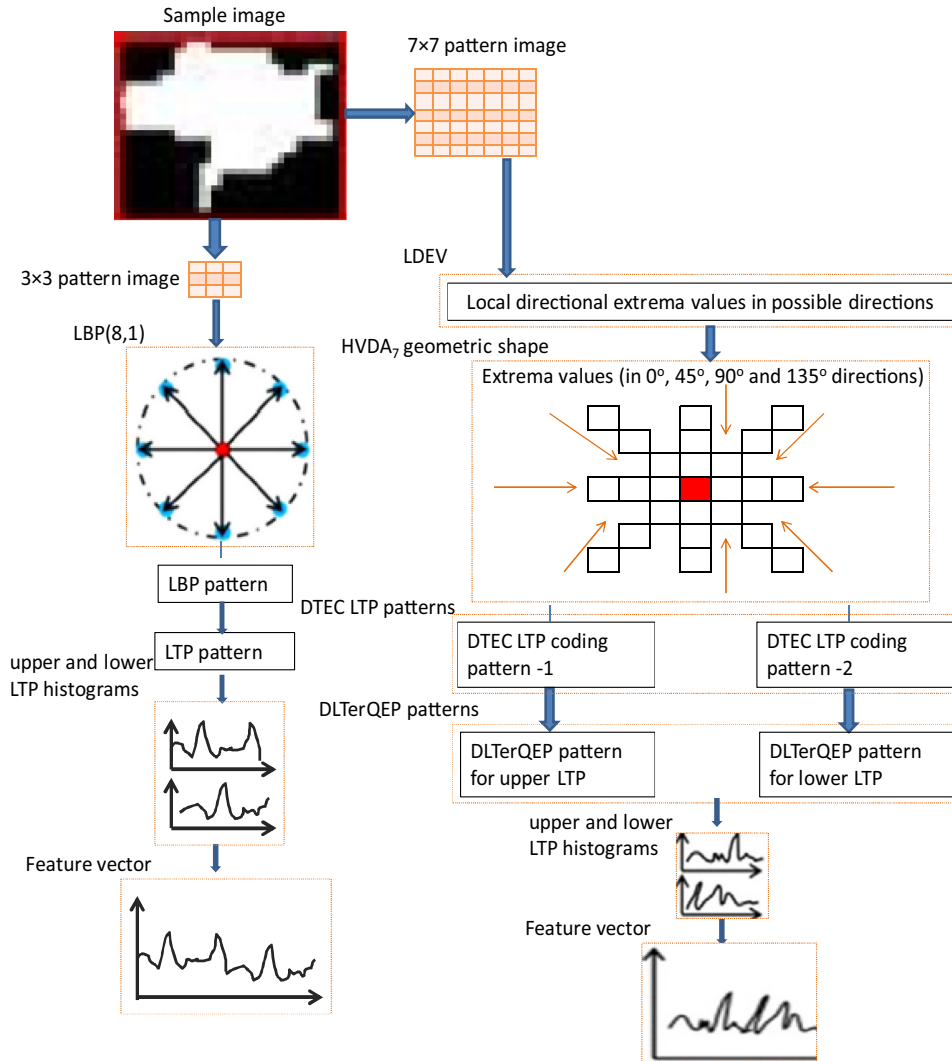
upper and lower
LTP histograms

Feature vector

Fig. 6. Procedure of feature extraction for DLTerQEP.

in the circle of radius $R(R > 0)$; 2^p binomial factor for each sign f_1 $(g_{p-}g_c)$.

A histogram is generated to represent the texture image after finding the *LBP* code of each pixel in the image. Fig. 1, shows the example of circular neighbor sets for different configurations of (P, R).

2.2. Local ternary patterns (LTPs)

Tan and Triggs [58] presented a new texture operator called local ternary pattern (*LTP*) which is the extension of *LBP*. They encoded the neighbor pixel values into 3-valued codes (Eq. (2))

Image
database

Query
image

QLTerQEP texture features

Calculate the LDEV
gray values in all
possible directions for
the local pattern
neighbourhoods of an
images

Directional LDEV in
HVDA$_7$ geometric
structure

LDEV values in 0° directions

LDEV values in 45° directions

LDEV values in 90° directions

LDEV values in 135° directions

Four directional ternary
extrema codings(DTEC)
at different thresholds
then analyze DLTerQEP
patterns

Retrieval

Similarity
measurement

Feature vector by
concatenating all
histograms
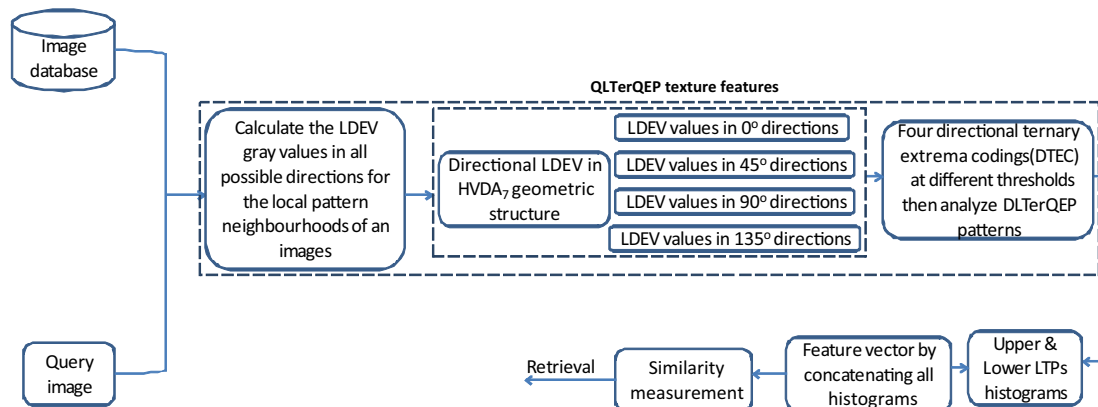
Upper &
Lower LTPs
histograms

**Fig. 7.** Flowchart of the proposed retrieval system framework.

Table 1
Data acquisition details of LIDC-IDRI-CT image database.

Case no.	Data	No. of slices	No. of images	Resolution	Slice thickness (mm)	Tube voltage (kv)	Tube current (mA)
1	LIDC-IDRI-0002	20	40	512 × 512	1.3 mm	120	440
2	LIDC-IDRI-0003	10	40	512 × 512	2.5 mm	120	300
3	LIDC-IDRI-0006	20	80	512 × 512	1.3 mm	120	440
4	LIDC-IDRI-0007	21	84	512 × 512	1.3 mm	120	440
5	LIDC-IDRI-0010	15	60	512 × 512	1.3 mm	120	401
6	LIDC-IDRI-0011	27	108	512 × 512	2.5 mm	120	265
7	LIDC-IDRI-0012	20	80	512 × 512	2.5 mm	120	300
8	LIDC-IDRI-0013	18	72	512 × 512	2.5 mm	120	320
9	LIDC-IDRI-0014	07	28	512 × 512	2.5 mm	120	300
10	LIDC-IDRI-0015	19	76	512 × 512	1.3 mm	120	361
11	LIDC-IDRI-0016	26	104	512 × 512	2.5 mm	120	265
12	LIDC-IDRI-0017	26	104	512 × 512	2.5 mm	120	265

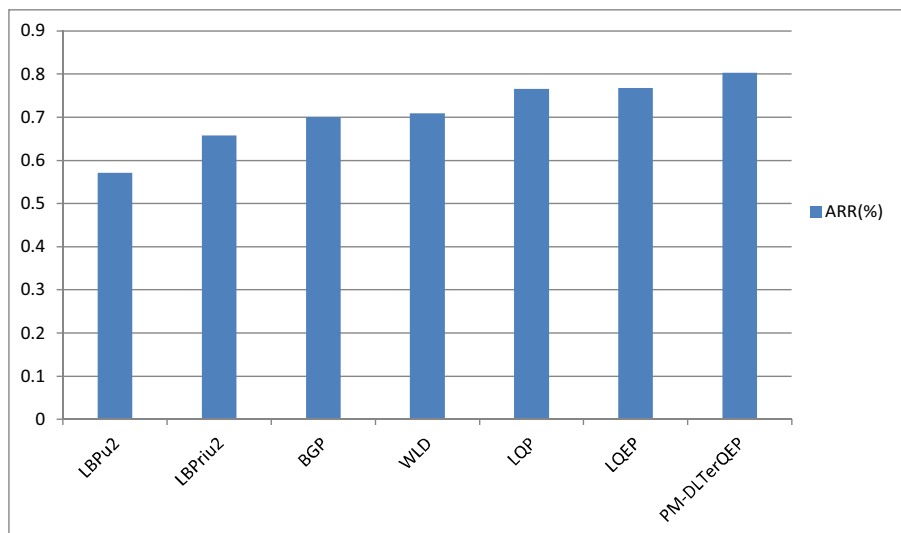URL for download: https://cabig.nci.nih.gov/tools/NCIA [22].

Fig. 8. Sample nodule images from LIDC-IDRI-CT image database.
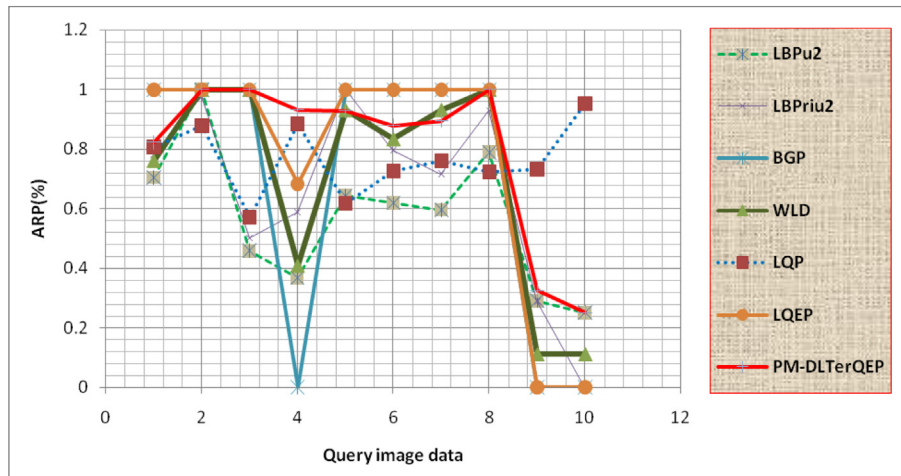
(a)

(b)

Fig. 9. Performance comparison of the proposed method (DLTerQEP) with other existing methods by passing different query images (1–10) in terms of: (a) ARP and (b) ARR on LIDC-IDRI-CT database.

instead of 2-valued codes of *LBP* by adding a user threshold. The mathematical value of the *LTP* can be expressed as follows:

$$\vec{f}(x, g_c, t) = \begin{cases} +1 & x \geqslant g_c + t \\ 0 & |x - g_c| < t \\ -1 & x \leqslant g_c - t \end{cases} \Bigg|_{x = g_p} \qquad (2)$$

In Eq. (2), upper pattern and lower pattern are constructed and coded because of thresholding step (*t*). As the result of which, $LTP_{8,2}$ will appear in the histogram of $3^8 = 6561$ bins which is a very large dimension and is split into a positive *LBP* code and a negative code as proposed by Tan and Triggs [58]. Binary *LBP* code replaced by a ternary *LTP* code (at threshold, *t* = 2) is shown in Fig. 2.

$$DTEC1(I(g_c))|_{\propto} = \begin{cases} \vec{f}_2(LDEV(g_{45}) \times LDEV(g_{43}), I(g_c)); \vec{f}_2(LDEV(g_{46}) \times LDEV(g_{42}), I(g_c)); \vec{f}_2(LDEV(g_{47}) \times LDEV(g_{41}), I(g_c)); \propto = 0° \\ \vec{f}_2(LDEV(g_{34}) \times LDEV(g_{54}), I(g_c)); \vec{f}_2(LDEV(g_{24}) \times LDEV(g_{64}), I(g_c)); \vec{f}_2(LDEV(g_{14}) \times LDEV(g_{74}), I(g_c)); \propto = 45° \\ \vec{f}_2(LDEV(g_{35}) \times LDEV(g_{53}), I(g_c)); \vec{f}_2(LDEV(g_{26}) \times LDEV(g_{62}), I(g_c)); \vec{f}_2(LDEV(g_{17}) \times LDEV(g_{71}), I(g_c)); \propto = 90° \\ \vec{f}_2(LDEV(g_{33}) \times LDEV(g_{55}), I(g_c)); \vec{f}_2(LDEV(g_{22}) \times LDEV(g_{66}), I(g_c)); \vec{f}_2(LDEV(g_{11}) \times LDEV(g_{77}), I(g_c)); \propto = 135° \end{cases} \qquad (5)$$

2.3. Local quantized extrema patterns (LQEPs)

Rao and Rao [52] have used the idea of local quantized pattern (*LQP*) [18] and directional local extrema pattern (*DLEP*) [36] to design the *LQEP* on natural image data sets for image retrieval. The *LQP* collects the directional geometric features from the given pattern of an image. Then, the extrema operation is performed on the directional geometric structures. Fig. 3 illustrates the example of *LQEP* feature calculation using $HVDA_7$ of possible directional *LQP* geometric structures for a given 7×7 pattern of an image.

In this paper, for a given center pixel (g_c) in an image *I*, the $HVDA_7$ geometric structure is collected for feature extraction using Fig. 3. The *LQEP* is defined as follows:

$$LQEP = [DE(I(g_c))|_{0°}, DE(I(g_c))|_{45°}, DE(I(g_c))|_{90°}, DE(I(g_c))|_{135°}] \qquad (3)$$

The more details about *LQEP* are available in the paper of Rao and Rao [52].

2.4. Directional local ternary quantized extrema patterns (DLTerQEPs)

The idea of local patterns (the *LBP*, the *LTP*, and the *LQEP*) has been adopted to define directional local ternary quantized extrema pattern (*DLTerQEP*). *DLTerQEP* describes the spatial structure of the local texture in ternary patterns using the local extrema and directional geometric structures.

In the proposed *DLTerQEP* for a given image, the local extrema in all directions is acquired by computing local difference between the center pixel and its neighbours by indexing of the patterns with pixel positions. The positions are indexed in a manner to write the four directional extremas operator calculations. Local directional extrema values (*LDEV*) for the local pattern neighbourhoods of an image (*I*) are calculated as follows:

$$LDEV(q, r) = \sum_{q=1}^{k_1} \sum_{r=1}^{k_1} [I(q, r) - I(1 + floor(k_1/2), 1 + floor(k_1/2))] \qquad (4)$$

where the size of input image is $k_1 \times k_1$.

Four directional, $HVDA_7$ geometric structure of possible directional *LQP* geometries is used for feature extraction. Directional local extrema values in 0°, 45°, 90° and 135° directions are extracted in the shape of $HVDA_7$ from *LDEV* values as calculated by Eq. (4). Then four directional ternary extrema codings (*DTEC*) are collected based on the four directions (0°, 45°, 90° and 135°) at different thresholds using the concept of *LTP* given in Eq. (2). The ternary coding patterns are obtained as follows:

where $LDEV(g_{ab}) = LDEV$ at (a, b) *position of* 7×7 grid and g_c denotes the gray value of the center pixel.

For upper *LTP*, *DTEC1* is computed from Eq. (5) by obtaining value of $\vec{f}_2$ as follows:

$$\vec{f}_2(x, g_c) = \begin{cases} 1, & \text{if}(x \geqslant (\text{threshold} = 2)); \\ 0, & \text{if}(x < (\text{threshold})); \end{cases} \qquad (6)$$

Similarly, from above Eq. (5), lower *LTP*, *DTEC2* is computed by obtaining value of $\vec{f}_2$ as follows:

$$\vec{f}_2(x, g_c) = \begin{cases} 1, & \text{if}(x \leqslant (\text{threshold} = -2)); \\ 0, & \text{if}(x > (\text{threshold})); \end{cases} \qquad (7)$$

The *DTEC* is defined from the Eqs. (5)–(7) as follows:

$$DTEC(I(g_c)) = \begin{bmatrix} DTEC1(I(g_c))|_{0°}, DTEC1(I(g_c))|_{45°}, DTEC1(I(g_c))|_{90°}, DTEC1(I(g_c))|_{135°}; \\ DTEC2(I(g_c))|_{0°}, DTEC2(I(g_c))|_{45°}, DTEC2(I(g_c))|_{90°}, DTEC2(I(g_c))|_{135°} \end{bmatrix} \qquad (8)$$

As above *DTEC* coding is converted into two binary codes (upper *LTP* code and lower *LTP* code) as that in the *LTP*. So in practice, *DLTerQEP* allows concatenation of four directional extremas for *P* = 12-bit ($w = 0...11$) binary coding string generation (3-bit from each given directional extrema) in each binary pattern of *LTP*.

Now, by multiplying with the binomial weights to each *DTEC LTP* coding, the unique *DLTerQEP* values (decimal values) for a particular given pattern (7×7) for characterization of spatial structure of the local pattern are defined by Eq. (9).

$$DLTerQEP_{\alpha, P} = \sum_{w=0}^{P-1} DTEC_{(\text{upper/lower}), w} 2^w \qquad (9)$$

For whole image, each *DTEC LTP* (upper and lower) map from above is with values ranging from 0 to 4095 (0 to $2^P - 1$), so complete *DTEC LTP* map is built with values ranging from 0 to

8191 (0 to $((2(2^P)) - 1)$. The complete image is represented by constructing a histogram using the following Eqs. (10) and (11) after detecting the local pattern, PTN (LBP or LTP or $DTEC$ or $DLTerQEP$).

$$H^1_{DLTerQEP}(v) = (1/(k_1 \times k_1)) \sum_{q=1}^{k_1} \sum_{r=1}^{k_1} f_3(DLTerQEP_{upper}(q,r), v);$$

$$v \in [0, 4095]; \tag{10}$$

$$f_3(x, y) = \begin{cases} 1, & \text{if}(x = y); \\ 0, & \text{if}(x \neq y); \end{cases}$$

$$H^2_{DLTerQEP}(v) = (1/(k_1 \times k_1)) \sum_{q=1}^{k_1} \sum_{r=1}^{k_1} f_4(DLTerQEP_{lower}(q,r), v); \tag{11}$$

$$v \in [0, 4095];$$

Other parameter specifications of Eq. (11) are same as in Eq. (10),

$$H_{DLTerQEP}(v) = [H^1_{DLTerQEP}(v), H^2_{DLTerQEP}(v)] \tag{12}$$

As we know that LTP is affected with the large size of feature dimensions (from 2^P to 3^P) as in Eq. (2) (using 3-value ternary coding). In this paper using user thresholds, it has been studied that Tan and Triggs [58] solved the above said problem by converting the ternary pattern into two binary patterns (upper LTP and lower LTP) (see in Eqs. (6) and (8)). It is also reported in Liao [29] and Yeffet and Wolf [68] that the original LTP operator is inferior due to the disintegration of LTP as upper and lower $LBPs$. The best performance with the reasonable feature dimension is considered, in this paper. An example of $DLTerQEP$ calculation for a center pixel (gray value "1") marked with the red color of a given 7×7 pattern of an image has been illustrated in Fig. 4.

The proposed $DLTerQEP$ is disparate from the familiar method LBP. The $DLTerQEP$ extracts the spatial relation between any pair of neighbors in a local region along the given directions, while LBP extracts relation between the center pixel and its neighbors. $DLTerQEP$ take out the directional edge information based on local extrema that differ it from the existing LBP. Therefore, $DLTerQEP$ captures more spatial information as compared with LBP. $DLTerQEP$ also provides a significant increase in discriminative power by allowing larger local pattern neighborhoods.

Fig. 5 illustrates the responses obtained by applying the LBP, the LTP, the $LQEP$ and the $DLTerQEP$ on a reference face image. Face image is chosen as it provides the results which are visibly comprehensible to differentiate the effectiveness of these approaches. It is monitored that the feature map of $DLTerQEP$ (upper and lower $LTPs$) operator is able to capture more directional edge information as compared to feature map of LBP, LTP and $LQEP$ for texture extraction.

3. Feature extraction and framework of proposed method

3.1. Feature extraction

Fig. 6 illustrates the procedure of feature extraction based on $DLTerQEP$ and stepwise algorithm used for same is given below:

Algorithm. Input: Query image;
Output: Retrieval results

Table 3
Performance comparison of the (DLTerQEP) with other existing methods in terms of ARR on LIDC-IDRI-CT database.

	LBPu2	LBPriu2	BGP	WLD	LQP	LQEP	PM-DLTerQEP
ARR	0.5717	0.6582	0.7000	0.7089	0.7654	0.7683	**0.8033**

PM: Proposed method i.e., DLTerQEP.
Bold values are showing the best performance value by the proposed descriptor in the table.

1. Load the query image (or gray-scale image).
2. Calculate local directional extrema values ($LDEV$) in all possible directions.
3. Collect directional extrema values at 0°, 45°, 90° and 135° directions in $HVDA_7$ geometric structure for a given center pixel.
4. Compute four directional ternary extrema codings ($DTEC$) (for upper LTP and lower LTP) (12-bit binary string in each part of LTP of $DTEC$ coding).
5. Compute the $DLTerQEP$ decimal values for upper and lower $LTPs$.
6. Draw the histogram for each 12-bit $DLTerQEP$.
7. Construct a feature vector by concatenating all histograms.
8. Compare the query image with the image in the database using Eq. (13).
9. Retrieve the images based on the best matches.

3.2. Proposed system framework

Figs. 6 and 7 illustrate the feature extraction procedure and DLTerQEP flowchart of proposed retrieval system framework respectively.

3.3. Similarity measure

The representation of feature vector of query image Q is $f_Q = (f_{Q_1}, f_{Q_2}, \ldots, f_{Q_{L_g}})$ acquired after the feature extraction. Likewise, dataset $|DB|$ of all medical images is represented with feature vectors $f_{DB_j} = (f_{DB_{j1}}, f_{DB_{j2}}, \ldots, f_{DB_{jL_g}}); j = 1, 2, \ldots, |DB|$. However, only purpose here is to obtain n top match images by measuring the distance between query image and image in the dataset $|DB|$. Finally, n best images are displayed that are similar to the query image.

In this paper, d_1 distance measure is used as similarity distance metrics and this is shown below:

$$D(Q, DB) = \sum_{i=1}^{L_g} \left| \frac{f_{DB_{ji}} - f_{Q,i}}{1 + f_{DB_{ji}} + f_{Q,i}} \right| \tag{13}$$

where $f_{DB_{ji}}$ is the ith feature of the jth image in the database $|DB|$.

3.4. Evaluation measures (adopted from [Murala and Jonathan [33]])

The performance of the proposed method is measured in terms of precision, average precision or average retrieval precision (ARP), recall, average recall, and average retrieval rate (ARR).

For the query image I_q, the precision (P) and recall (R) are defined as follows:

$$Precision : P(I_q) = \frac{\text{Number of relevant images retrieved}}{\text{Total number of images retrieved}} \tag{14}$$

Table 2
Performance of DLTerQEP in terms of ARR with different thresholds for ternary value calculation on LIDC-IDRI-CT image database.

Method	Threshold (t)									
	1	2	3	4	5	6	7	8	9	10
DLTerQEP	.7989	.8031	**.8033**	.8021	.8003	.7997	.7994	.7973	.7971	.7909

Bold values are showing the best performance value by the proposed descriptor in the table.

$$ARP = \frac{1}{|DB|}\sum_{i=1}^{|DB|} P(I_i)|_{n\leqslant 10} \qquad (15)$$

$Recall : R(I_q)$

$$= \frac{\text{Number of relevant images retrieved}}{\text{Total number of relevant images in the database}} \qquad (16)$$

$$ARR = \frac{1}{|DB|}\sum_{i=1}^{|DB|} R(I_i)|_{n\geqslant 10} \qquad (17)$$

3.5. Abbreviations

The abbreviations used in the analysis of results are:

LBP: *Local binary patterns* as defined in Ojala et al. [46] and Ojala et al. [47].
LBPu2_P_R: *LBP* with uniform patters at (*P* = 8,16,24, and *R* = 1,2,3 respectively) neighborhood size.
LBPriu2: *LBP* rotational invariant uniform patterns.
INTH: *Intensity histogram* as defined in Sørensen et al. [55].

Table 4
Data acquisition details of VIA/I-ELCAP-CT lung image database.

Data	No. of slices	Resolution	In-plane resolution	Slice thickness (mm)	Tube voltage (kv)
W1-10	100	512×512	0.76×0.76	1.25	120

URL for download: http://www.via.cornell.edu/-databases/lungdb.html.

GLCM1: *Gray level cooccurrence matrix Type 1* (*Autocorrelation*) as also defined in Sørensen et al. [55].
GLCM2: *Gray level cooccurrence matrix Type 2* (*Correlation*) as also defined in Sørensen et al. [55].
BGP: *Binary gabor patterns* as defined in Zhang et al. [72].
WLD: *Weber law descriptor* as defined in Chen et al. [5].
LQP: *Local quinary patterns* as defined in Nanni et al. [43].
CS_LBP: *Circular symmetric local binary patterns* as defined in Heikkila et al. [17].
BLK_LBP: *Block based LBP* as defined in Takala et al. [56].
DBWP: *Directional binary wavelet patterns* as defined in Murala et al. [35].
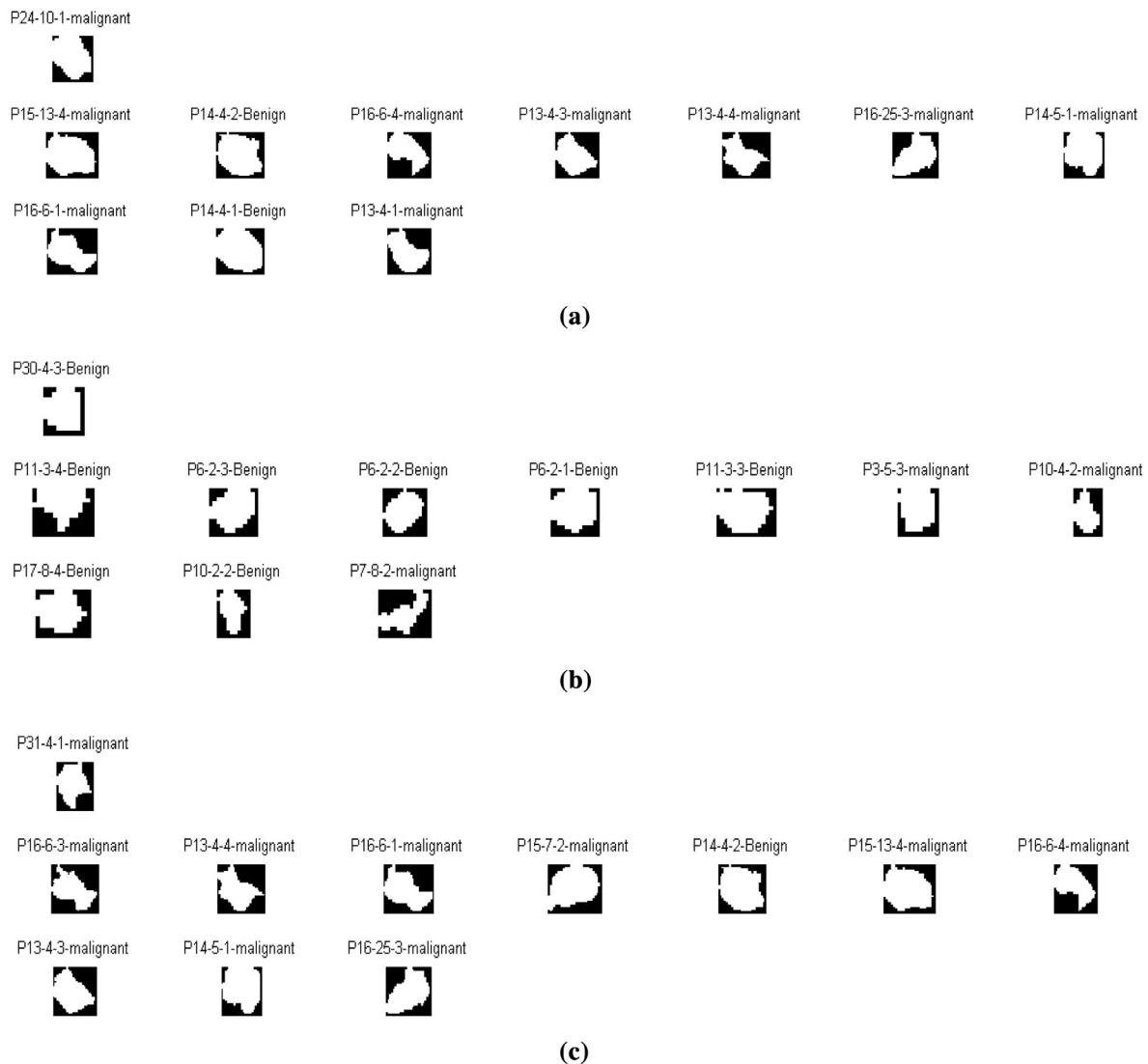DLEP: *Directional local extrema patterns* as defined in Murala et al. [36].

Fig. 10. Query results of DLTerQEP on LIDC–IDRI-CT database by passing three query images.
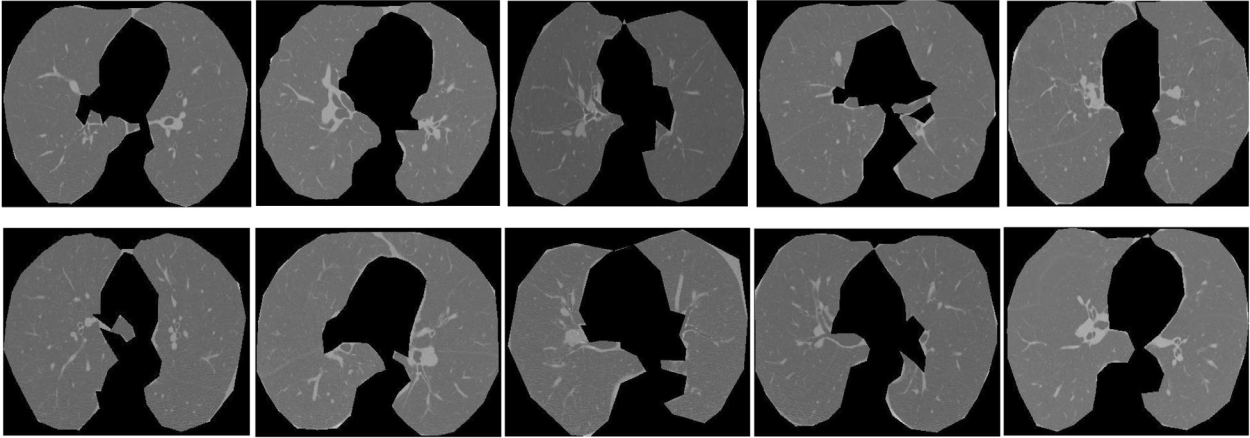
Fig. 11. Sample images from VIA/I-ELCAP-CT image database.

LDP: *Local derivative patterns* as defined in Zhang et al. [71].
LTP: *Local ternary patterns* as defined in Tan and Triggs [58].
LTCoP: *Local ternary co-occurrence patterns* as defined in Murala and Jonathan [33].
LMeP: *Local mess patterns* as defined in Murala and Jonathan [34].

LMePu2: *LMeP* with uniform patterns.
LQEP: *Local quantized extrema patterns* as defined in Rao and Rao [52].
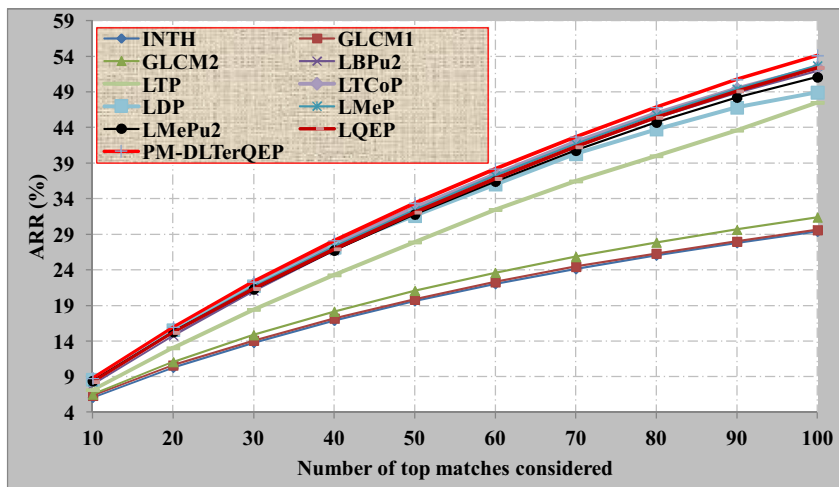DLTerQEP: *Directional local ternary quantized extrema patterns* (PM – proposed method).
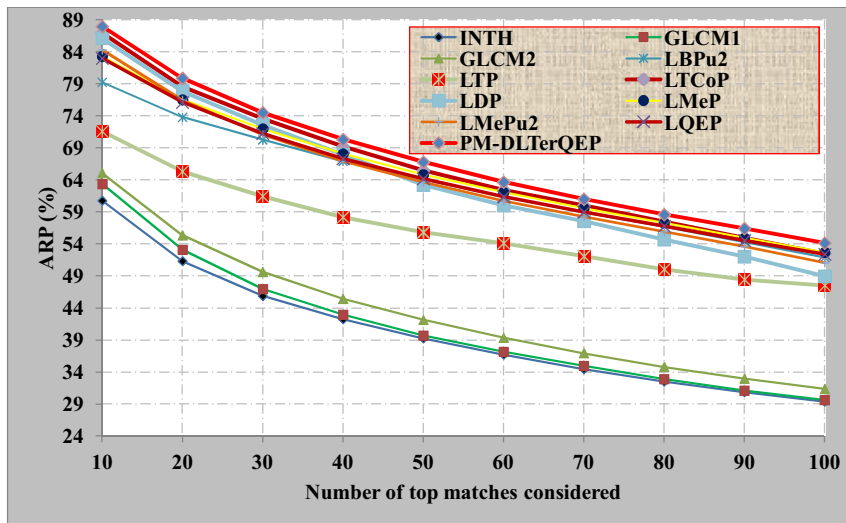
(a)

Fig. 12. Comparison of the DLTerQEP with other existing methods in terms of: (a) ARP and (b) ARR on VIA/IELCAP-CT database.

Table 5
Performance of DLTerQEP in terms of recall with different thresholds for ternary value calculation on VIA/I-ELCAP-CT database.

| Method	Threshold (t)									
	1	2	3	4	5	6	7	8	9	10
DLTerQEP	53.36	54.07	54.10	**54.13**	54.03	53.97	53.89	53.76	53.68	53.51

Bold values are showing the best performance value by the proposed descriptor in the table.
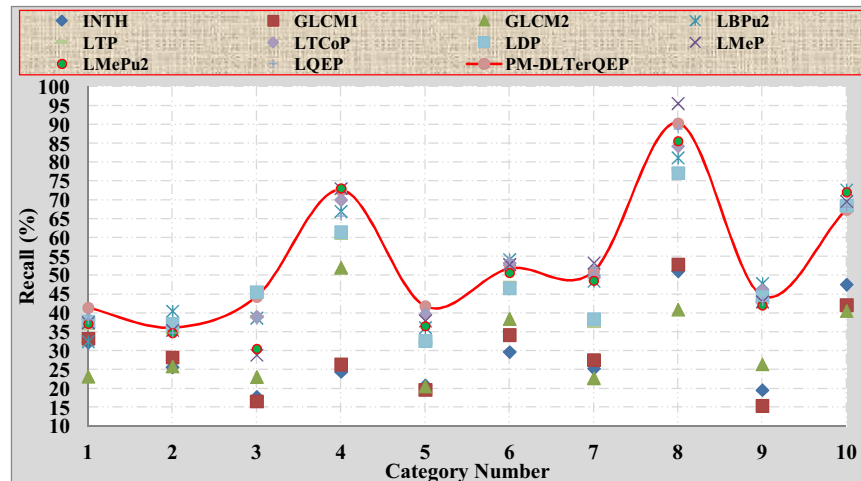
Table 6
Group wise performance of the proposed method and other existing methods in terms of recall values on VIA/I-ELCAP-CT database.

Method	INTH	GLCM1	GLCM2	LBPu2	LTP	LTCoP	LDP	LMeP	LMePu2	LQEP	PM-DLTerQEP
Group											
1	32.2	33.23	23.15	32.44	36.05	38.4	37.73	37.43	37.18	38.23	**41.41**
2	25.63	28.27	25.84	40.5	34.87	36.03	37.14	35.45	34.7	34.78	**36.12**
3	17.79	16.57	23.08	38.67	39.11	38.99	45.59	28.9	30.5	38.76	**44.33**
4	24.43	26.38	52.05	66.95	59.94	70.01	61.49	72.97	73.07	65.79	**72.58**
5	20.79	19.65	20.55	36.17	32.11	39.67	32.64	37.93	36.55	40.29	**41.82**
6	29.68	34.19	38.47	54.24	48.09	53.22	46.61	52.9	50.63	54.15	**51.77**
7	25.3	27.56	22.78	48.49	36.54	49.45	38.4	53.27	48.57	52.08	**51.00**
8	51.06	52.9	40.93	81.18	78.24	84.23	77.11	95.56	85.57	88.79	**90.29**
9	19.57	15.42	26.41	47.84	43.11	46.09	44.24	42.96	42.04	43.11	**44.63**
10	47.57	42.1	40.57	72.67	67.19	68.57	68.55	69.58	72.03	68.08	**67.39**
Total	29.4	29.63	31.38	51.915	47.53	52.47	48.95	52.7	51.08	52.41	**54.13**

Bold values are showing the best performance value by the proposed descriptor in the table.
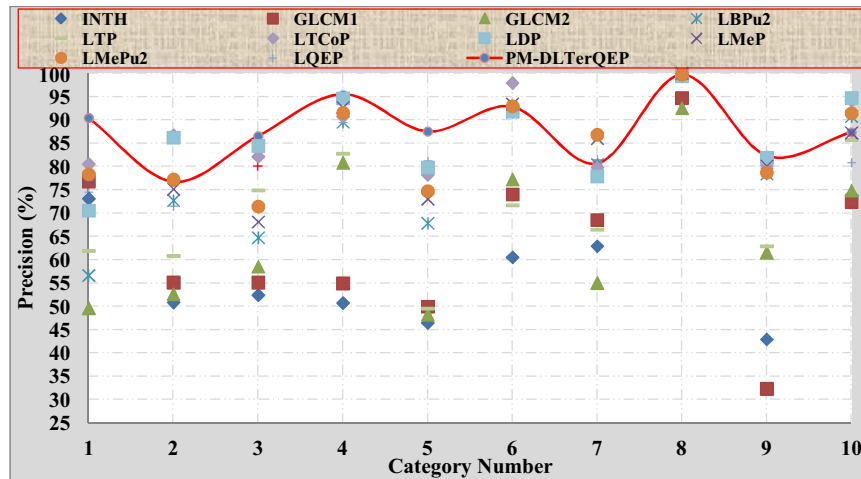
Fig. 13. Categorywise performance of DLTerQEP and other existing methods in terms of: (a) precision and (b) recall on VIA/I-ELCAP-CT database.

Table 7
MRI data acquisition details (adopted from [Marcus et al. [32]]).

Sequence	MP-RAGE
TR (msec)	9.7
TE (msec)	4.0
Flip angle (°)	10
TI (ms)	20
TD (ms)	200
Orientation	Sagittal
Thickness, gap (mm)	1.25, 0
Resolution (pixels)	176 × 208

URL for download: www.ncbi.nlm.nih.gov/pubmed/17714011.

4. Experimental results and discussions

The performance of the proposed algorithm is analyzed for biomedical image retrieval by conducting experiments on three different medical databases. The results yielded by the proposed method are examined in the following subsections.

In all the experiments, each image in the database is chosen as the query image. For each query image, the system collects n database images $X = (x_1, x_2, ..., x_n)$, with the shortest image matching distance (Eq. (13)). If x_i, $i = 1, 2, ..., n$ associate with the same category of the query image, we can say that the system has correctly matched the desired. In this paper, we examined the impact of different values of thresholds (t) in Eqs. (6) and (7) for ternary values calculation and fixed the (t) value which gives the better retrieval performance in terms of average retrieval precision (*ARP*) and average retrieval rate (*ARR*).

4.1. Experiment on LIDC-IDRI-CT data set

Experiments are conducted on the images collected from Lung Image Database Consortium and Image Database Resource Initiative (*LIDC-IDRI*), which is public lung image database of *CT* scans as been provided by Kascic and NEMA-CT image database [45]. The database is separated into 84 cases, each containing around 100–400 Digital Imaging and Communication (*DICOM*) images and an *XML* data file containing the physicians annotations. Database contains 143 nodules having size range of 3 to 30 mm (to

be manually segmented by radiologists). The *CT* lung images (512 × 512) from the database are converted into 'tif' image format for rapid processing with the use of Lampert [28]. Radiologists detected the locations of nodules which have also been provided. Furthermore, *ROIs* were annotated manually from each slice from some patients to construct the *ROI CT* image database. For the experiment, 12 patient cases consisting of 75 nodules (26 benign and 49 malignant) and 229 slices have been selected. The *CT* scan data acquisition details are given in Table 1. Fig. 8 depicts the sample lung nodule images of *LIDC-IDRI-CT* database (one image from each patient scan).

The performance of the proposed method is measured in terms of *ARP* and *ARR* as shown in Fig. 9 and Table 3. The Fig. 9 shows the retrieval performance for top ten matches of the proposed method (*DLTerQEP*) and some other existing methods (*LBPu2, LBPriu2, BGP, WLD, LQP, LQEP*) in terms of *ARP* and *ARR* by passing different query images (1–10) on *LIDC-IDRI-CT* database. Table 2 summarizes the performance of the proposed method (*DLTerQEP*) in terms of *ARR* with different thresholds for ternary value calculation on *LIDC-IDRI-CT* database. From Table 2, it is observed that the threshold '3' is showing better performance for *DLTerQEP*. Table 3 summarizes the performance of different methods in terms of *ARR*. The Fig. 10 shows that *DLTerQEP* achieves better performance over the existing methods *LBP, BGP, WLD, LQP* and *LQEP* on most of the cases. Fig. 10 illustrates three query results of the proposed method (*DLTerQEP*) by considering ten top matches on *LIDC-IDRI-CT* database.

4.2. Experiment on VIA/I-ELCAP-CT data set

To perform the evaluation of different computer-aided detection systems, computer tomography (*CT*) dataset is designed by vision and image analysis (*VIA*) group and international early lung cancer action program (*I-ELCAP*) [62]. *DICOM* format is used to store these images. A 1.25-mm slice thickness is acquired in a single breath hold with the *CT* scans. The radiologist also given the locations of nodules detected by them. So, the *ROI CT* image database is produced from manually annotated *ROIs*. Table 4 shows the experiments on date acquisition details of *CT* scans of about 10 scans having 100 images each of resolution 512 × 512. Fig. 11
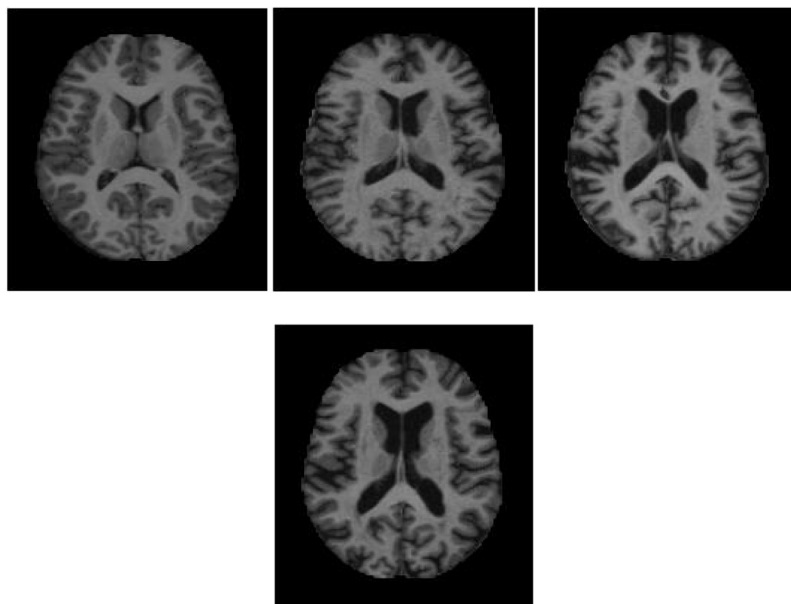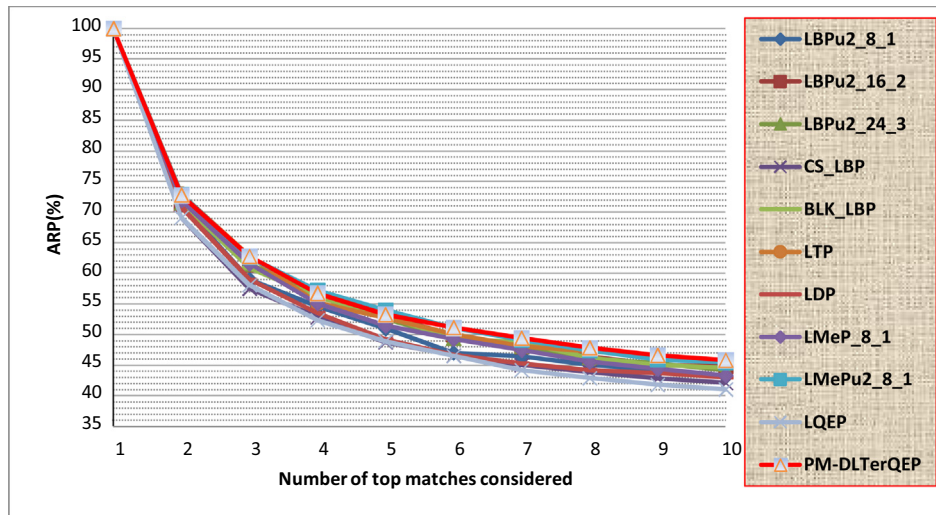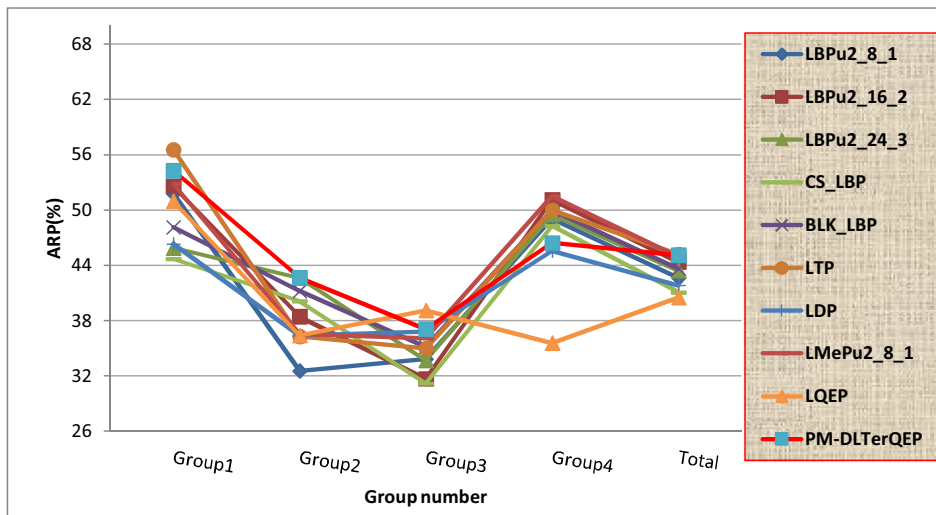

Fig. 14. Sample images from OASIS-MRI database.

(a)

(b)

Fig. 15. (a) Comparison of proposed method with other existing methods as function of number of top matches and (b) different group of images (based on the shape of ventricular in the images) comparison of proposed method with other existing methods on OASIS-MRI database.

represents the sample images of *VIA/I-ELCAP* database (one image from each category).

Fig. 12 illustrates the retrieval performance of the proposed method (*DLTerQEP*) and other existing methods (*INTH, GLCM1, GLCM2, LBPu2, LTP, LTCoP, LDP, LMeP, LMePu2, LQEP*) in terms of *ARP* and *ARR*. Table 5 summarizes the performance of the proposed method (*DLTerQEP*) in terms of recall with different thresholds for ternary value calculation on *VIA/I-ELCAP* database. From Table 5, it is observed that the threshold '4' is showing better performance for *DLTerQEP*. Table 6 shows the group wise performance of the proposed method and other existing methods in terms of recall on *VIA/I-ELCAP-CT* database. Fig. 13 illustrates the individual category performances of the proposed method and other existing methods

in terms of precision and recall. From Figs. 12 and 13, it is clear that the proposed method (*DLTerQEP*) outperforms other existing methods in terms of precision, recall, *ARP*, and *ARR* on *VIA/I-ELCAP-CT* database.

4.3. Experiment on OASIS-MRI data set

In the experimentation, the open access series of imaging studies (*OASIS*) database is utilized. Marcus et al. [32] constructed the open access series of imaging studies (*OASIS*) that is a series of magnetic resonance imaging (*MRI*) dataset. (dataset is available online for use in medical research field). Table 7 presents the details of *MRI* acquisition. A cross-sectional collection of 421

Table 8
Performance of DLTerQEP with different thresholds for ternary value calculation on OASIS-MRI database.

Method	Threshold (*t*)									
	1	2	3	4	5	6	7	8	9	10
DLTerQEP	43.68	43.19	44.41	43.71	44.05	44.74	44.75	**45.10**	44.85	44.73

Bold values are showing the best performance value by the proposed descriptor in the table.

patients aged between 18 and 96 years exists in this data set. Furthermore, based on the shape of ventricular in the images, four categories (124, 102, 89, and 106 images) from 421 images are grouped to evaluate the retrieval of images. Fig. 14 represents the one sample image from each category of *OASIS* database.

Table 9 summarizes the retrieval results of *DLTerQEP* and other existing methods on *OASIS* database in terms of *ARP*. The following inference is drawn in terms of *ARP* at $n = 10$ from Table 6 and Fig. 15:

(1) The average retrieval precision of proposed directional pattern method (*DLTerQEP* (45.10%)) is higher as compared to *LBPu2_8_1* (42.63%), *LBPu2_16_2* (44.37%), *LBPu2_24_3* (43.44%), *CS_LBP* (41.06%), *BLK_LBP* (43.63%), *LDP* (41.8%), *LMePu2_8_1* (44.96%) and *LQEP* (40.51%).
(2) The average retrieval precision of proposed directional pattern method is slightly less than *LTP* (45.17%) but as we see the results on the most of cases, proposed method has shown very good performance.

Fig. 15(a) shows the graphs depicting the retrieval performance of the proposed method and other existing methods in terms of *ARP* as function of number of top matches. Fig. 15(b) illustrates the group wise performance of various methods in terms of *ARP* on *OASIS-MRI* image database. Table 8 summarizes the performance of the proposed method (*DLTerQEP*) with different thresholds for ternary value calculation on *OASIS-MRI* database. From Table 8, it is observed that the threshold '8' is showing better performance for *DLTerQEP*. From Fig. 15, it is evident that the proposed method outperforms the many of other existing methods on *OASIS-MRI* image database for biomedical image retrieval.

4.4. Feature vector length v/s performance

Table 10 shows the feature vector length for a given query image using *LBP*, *LBPu2*, *LTP*, *LTCoP*, *DBWP*, *LDP*, *LMeP*, *LMePu2*, *DLEP*, *LQEP* and *DLTerQEP*. The experimentation is carried out on core2 Quad computer with 2.66 GHz, 4 GB of memory and all methods are implemented on the *MATLAB* software. From the Table 10, it is clear that the feature vector length of proposed method (*DLTerQEP*) is more as compared to other existing methods, as it outperforms in terms of *ARP* and *ARR* on three different biomedical databases.

5. Conclusions and future perspectives

In this paper, a new descriptor named directional local ternary quantized extrema pattern (*DLTerQEP*) is proposed for medical image indexing and retrieval. The *DLTerQEP* extracts the ternary relationship among the neighbors for a given center pixel in the selected *LQP* structural pattern of directional local extrema values. To test the robustness and effectiveness of the proposed algorithm, results are taken on three different types of benchmark medical databases. The detailed investigations of the results show a significant improvement of the proposed method in terms of *ARP* and *ARR* as compared to *LBP*, *LTP*, *LQEP* and other state-of-the-art methods on *LIDC-IDRI-CT*, *OASIS-MRI* and *VIA/I-ELCAP-CT* databases.

This work will be useful in other applications of content based image indexing and retrieval. The performance of the proposed method with ternary coding can also be further checked by replacing with other non-binary coding scheme such as local quinary coding. The generality of the proposed descriptor was validated across three different types of benchmark biomedical databases. In future experiments, the proposed descriptor can be compared in dozens of biomedical or ordinary datasets against state of the art descriptors.

Acknowledgments

Table 9
Comparison of various techniques showing group wise performance in terms of precision on OASIS-MRI database.

Method	Precision (%) ($n = 10$)				
	Group1	Group2	Group3	Group4	Total
LBPu2_8_1	51.77	32.54	33.82	49.06	42.63
LBPu2_16_2	52.58	38.43	31.68	51.13	44.37
LBPu2_24_3	45.88	42.64	33.7	49.53	43.44
CS_LBP	44.7	40.1	31.17	48.27	41.06
BLK_LBP	48.13	41.22	35.16	50.01	43.63
LTP	56.53	36.27	34.97	50	45.17
LDP	46.29	36.37	36.82	45.56	41.8
LMePu2_8_1	52.82	36.56	36.08	51.50	44.96
PM-DLTerQEP	**54.27**	**42.65**	**37.08**	**46.42**	**45.10**

Bold values are showing the best performance value by the proposed descriptor in the table.

Table 10
Feature vector length of query image using various methods.

Method	Feature vector length
LBP	256
LBPu2	59
LTP	2×256
LTCoP	2×256
DBWP	$8 \times 10 \times 256$
LDP	4×256
LMeP	3×256
LMePu2	3×59
DLEP	4×512
LQEP	1×4096
DLTerQEP	2×4096

References

[1] T. Ahonen, A. Hadid, M. Pietikainen, Face description with local binary patterns: application to face recognition, IEEE TPAMI 28 (12) (2006) 2037–2041.
[2] S. Antani, L.R. Long, G.R. Thoma, Content-based image retrieval for large biomedical image archives, in: Proc 11th World Cong Medical Informatics, 2004, pp. 829–833.
[3] A. Bala, T. Kaur, Local texton XOR patterns: a new feature descriptor for content based image retrieval, Eng. Sci. Technol.: Int. J. 19 (2016) 101–112.
[4] J. Chen, V.P. Kellokumpu, G. Zhao, M. Pietikäinen, RLBP: Robust local binary pattern, in: Proc. the British Machine Vision Conference (BMVC 2013), Bristol, UK, 2013.
[5] J. Chen, S. Shan, C. He, G. Zhao, M. Pietikäinen, X. Chen, W. Gao, WLD: a robust local image descriptor, IEEE Trans. Pattern Anal. Mach. Intell. 32 (9) (2009) 1705–1720.
[6] M.N. Do, M. Vetterli, Wavelet-based texture retrieval using generalized Gaussian density and Kullback-leibler distance, IEEE Trans. Image Process. 11 (2) (2002) 146–158.
[7] S.R. Dubey, S.K. Singh, R.K. Singh, Local bit-plane decoded pattern: a novel feature descriptor for biomedical image retrieval, IEEE J. Biomed. Health Inform. PP (99) (2015) 1.
[8] S.R. Dubey, S.K. Singh, R.K. Singh, Local diagonal extrema pattern: a new and efficient feature descriptor for CT image retrieval, IEEE Signal Process. Lett. 22 (9) (2015) 1215–1219.
[9] S.R. Dubey, S.K. Singh, R.K. Singh, Local wavelet pattern: a new feature descriptor for image retrieval in medical CT databases, IEEE Trans. Image Process. 24 (12) (2015) 5892–5903.
[10] J.C. Felipe, A.J.M. Traina, C.J. Traina, Retrieval by content of medical images using texture for tissue identification, in: Proceedings of the 16th IEEE Symposium on Computer-Based Medical Systems, New York, USA, 2003, pp. 175–180.
[11] P. Gibbs, L.W. Turnbull, Textural analysis of contrast-enhanced MR images of the breast, Magn. Reson. Med. 50 (1) (2003) 92–98.

[12] Y. Guo, G. Zhao, M. Pietikäinen, Local configuration features and discriminative learnt features for texture description. Chapter: Local binary patterns: new variants and applications, Stud. Comput. Intell. 506 (2013) 113–129.

[13] Z. Guo, L. Zhang, D. Zhang, Rotation invariant texture classification using LBP variance with global matching, Pattern Recogn. 43 (3) (2010) 706–716.

[14] M. Hajek, M. Dezertova, A. Materka, R. Lerski (Eds.), Texture Analysis for Magnetic Resonance Imaging, Med4 Publishing, 2006, pp. 1–233.

[15] R. Haralick, Statistical and structural approaches to texture, Proc. IEEE 67 (5) (1979) 786–804.

[16] R. Haralick, K. Shanmugan, I. Dinstain, Textural features for image classification, IEEE Trans. Syst. Man Cybern. 3 (6) (1973) 610–622.

[17] M. Heikkila, M. Pietikainen, C. Schmid, Description of interest regions with local binary patterns, Pattern Recogn. 42 (2009) 425–436.

[18] S.U. Hussain, B. Triggs, Visual recognition using local quantized patterns, in: European Conference on Computer Vision (ECCV 2012), Part II, LNCS 7573, Italy, 2012, pp. 716–729.

[19] E. Irmak, E. Ergun Ercelebi, A.H. Ertas, Brain tumor detection using monomodal intensity based medical image registration and MATLAB, Turk. J. Electr. Eng. Comp. Sci. 24 (2016) 2730–2746.

[20] N. Jhanwara, S. Chaudhuri, G. Seetharamanc, B. Zavidovique, Content based image retrieval using motif co-occurrence matrix, Image Vis. Comput. 22 (14) (2004) 1211–1220.

[21] L. Jing, N.M. Allinson, A comprehensive review of current local features for computer vision, Neurocomput. Vis. Res. 71 (10–12) (2008) 1771–1787.

[22] E. Kascic, NBIA – National Cancer Imaging Archive NCIA (version 4.0): The NCI's Repository for DICOM-based Images. <https://cabig.nci.nih.gov/tools/NCIA>.

[23] A. Kassner, R.E. Thornhill, Texture analysis: a review of neurologic MR imaging applications, Am. J. Neuroradiol. 31 (5) (2010) 809–816.

[24] E.G. Keramidas, D.K. Iakovidis, D. Maroulis, N. Dimitropoulos, Thyroid texture representation via noise resistant image features, in: Proceedings of the 21st IEEE International Symposium on Computer based Medical Systems (CBMS 2008), 2008, pp. 560–565.

[25] M. Kokare, P.K. Biswas, B.N. Chatterji, Texture image retrieval using new rotated complex wavelet filters, IEEE Trans. Syst. Man Cybern. 33 (6) (2005) 1168–1174.

[26] M. Kokare, P.K. Biswas, B.N. Chatterji, Rotation-invariant texture image retrieval using rotated complex wavelet filters, IEEE Trans. Syst. Man Cybern. 36 (6) (2006) 1273–1282.

[27] M. Kokare, P.K. Biswas, B.N. Chatterji, Texture image retrieval using rotated wavelet filters, J. Pattern Recognit. Lett. 28 (2007) 1240–1249.

[28] T. Lampert, LIDC 2 Image Toolbox (Matlab). [Online]. Available: <https://wiki.cancerimagingarchive.net/display/Public/LungImageDatabaseConsortium>.

[29] W.H. Liao, Region description using extended local ternary patterns, in: Proceedings of 20th International Conference on Pattern Recognition (ICPR), 2010, pp. 1003–1006.

[30] L. Liu, Y. Long, P.W. Fieguth, S. Lao, G. Zhao, BRINT: binary rotation invariant and noise tolerant texture classification, IEEE Trans. Image Process. 23 (7) (2014) 3071–3084.

[31] W. Liu, H. Zhang, Q. Tong, Medical image retrieval based on nonlinear texture features, Biomed. Eng. Instrum. Sci. 25 (1) (2008) 35–38.

[32] D.S. Marcus, T.H. Wang, J. Parker, J.G. Csernansky, J.C. Morris, R.L. Buckner, Open access series of imaging studies (OASIS): cross sectional MRI data in young, middle aged, nondemented, and demented older adults, J. Cogn. Neurosci. 19 (9) (2007) 1498–1507.

[33] S. Murala, W.Q. Jonathan, Local ternary co-occurrence patterns: a new feature descriptor for MRI and CT image retrieval, Neurocomputing 119 (7) (2013) 399–412.

[34] S. Murala, W.Q. Jonathan, Local mesh patterns versus local binary patterns: biomedical image indexing and retrieval, IEEE J. Biomed. Health Inform. 18 (3) (2014) 929–938.

[35] S. Murala, R.P. Maheshwari, R. Balasubramanian, Directional binary wavelet patterns for biomedical image indexing and retrieval, J. Med. Syst. 36 (5) (2012) 2865–2879.

[36] S. Murala, R.P. Maheshwari, R. Balasubramanian, Directional local extrema patterns: a new descriptor for content based image retrieval, Int. J. Multimedia Inf. Retr. 1 (3) (2012) 191–203.

[37] S. Murala, R.P. Maheshwari, R. Balasubramanian, Local tetra patterns: new feature descriptor for content based image retrieval, IEEE Trans. Image Process. 21 (5) (2012) 2874–2886.

[38] L. Nanni, A. Lumini, Region Boost learning for 2D + 3D based face recognition, Pattern Recogn. Lett. 28 (15) (2007) 2063–2070.

[39] L. Nanni, A. Lumini, Local binary patterns for a hybrid fingerprint matcher, Pattern Recogn. 41 (11) (2008) 3461–3466.

[40] L. Nanni, A. Lumini, A reliable method for cell phenotype image classification, Artif. Intell. Med. 43 (2) (2008) 87–97.

[41] L. Nanni, A. Lumini, Ensemble of neural networks for automated cell phenotype image classification. Biomedical Image Analysis and Machine Learning Technologies: Applications and techniques (chapter in vision 2008), pp. 1–322, 2008.

[42] L. Nanni, S. Brahnam, S. Ghidoni, E. Menegatti, T. Barrier, Different approaches for extracting information from the co-occurrence matrix, PLoS ONE 8 (12) (2013), http://dx.doi.org/10.1371/journal.pone.0083554. e83554.

[43] L. Nanni, S. Brahnam, A. Lumini, A local approach based on a Local Binary Patterns variant texture descriptor for classifying pain states, Expert Syst. Appl. 37 (12) (2010) 7888–7894.

[44] L. Nanni, A. Lumini, S. Brahnam, Local binary patterns variants as texture descriptors for medical image analysis, Artif. Intell. Med. 49 (2) (2010) 117–125.

[45] NEMA-CT image database (Online). Available: <ftp://medical.nema.org/medical/Dicom/Multiframe/>, 2012.

[46] T. Ojala, M. Pietikainen, D. Harwood, A comparative study of texture measures with classification based on feature distributions, Pattern Recogn. 29 (1) (1996) 51–59.

[47] T. Ojala, M. Pietikainen, T. Maeenpaa, Multiresolution gray-scale and rotation invariant texture classification with local binary patterns, IEEE Trans. Pattern Anal. Mach. Intell. 24 (7) (2002) 971–987.

[48] A. Oliver, X. Lladó, J. Freixenet, J. Martí, False positive reduction in mammographic mass detection using local binary patterns, in: Proceedings of the Medical Image Computing and Computer Assisted Intervention (MICCAI 2007), Brisbane, Australia: Springer, Lecture Notes in Computer Science (LNCS) 4791, pp. 286–293, 2007.

[49] M. Paci, L. Nanni, A. Lahti, S.K. Aalto, J. Hyttinen, S. Severi, Non-binary coding for texture descriptors in sub-cellular and stem cell image classification, Curr. Bioinform. 8 (2) (2013) 208–219.

[50] P. Parida, N. Bhoi, Transition region based single and multiple object segmentation of gray scale images, Eng. Sci. Technol.: Int. J. 19 (3) (2016) 1206–1215.

[51] B. Ramamurthy, K.R. Chandran, V.R. Meenakshi, V. Shilpa, CBMIR: content based medical image retrieval system using texture and intensity for dental images, Commun. Comput. Inform. Sci. 305 (2012) 125–134.

[52] L.K. Rao, D.V. Rao, Local quantized extrema patterns for content-based natural and texture image retrieval, Hum. Centric Comput. Inform. Sci. (2015), http://dx.doi.org/10.1186/s13673-015-0044-z, 5(26).

[53] G. Scott, C.R. Shyu, Knowledge-driven multi dimensional indexing structure for biomedical media database retrieval, IEEE Trans. Inf. Technol. Biomed. 11 (3) (2007) 320–331.

[54] F.R. Siqueira, W.R. Schwartz, H. Pedrini, Multi-scale gray level co-occurrence matrices for texture description, Neurocomputing 120 (2013) 336–345.

[55] L. Sørensen, S.B. Shaker, M.D. Bruijne, Quantitative analysis of pulmonary emphysema using local binary patterns, IEEE Trans. Med. Imag. 29 (2) (2010) 559–569.

[56] V. Takala, T. Ahonen, M. Pietikainen, Block-based methods for image retrieval using local binary patterns. SCIA 2005, LNCS, 3450, pp. 882–891, 2005.

[57] H. Tamura, S. Mori, T. Yamawaki, Textural features corresponding to visual perception, IEEE Trans. Syst. Man Cybern. 8 (6) (1978) 460–473. SMC-8.

[58] X. Tan, B. Triggs, Enhanced local texture feature sets for face recognition under difficult lighting conditions, IEEE Trans. Image Process. 19 (6) (2010) 1635–1650.

[59] A. Traina, C. Castanon, C.J. Traina, Multiwavemed: a system for medical image retrieval through wavelets transformations, in: Proceedings of the 16th IEEE Symposium on Computer-Based Medical Systems, New York, USA, 2003, pp. 150–155.

[60] K. Vaidehi, T.S. Subashini, An intelligent content based image retrieval system for mammogram image analysis, J. Eng. Sci. Technol. 10 (11) (2015) 1453–1464.

[61] M. Verma, B. Raman, S. Murala, Local extrema co-occurrence pattern for color and texture image retrieval, Neurocomputing 165 (2015) 255–269.

[62] VIA/I-ELCAP CT Lung Image Dataset. Available (online) <http://www.via.cornell.edu/-databases/lungdb.html>.

[63] S.K. Vipparthi, S. Murala, A.B. Gonde, Local directional mask maximum edge patterns for image retrieval and face recognition, IET Comput. Vision 10 (3) (2016) 182–192.

[64] S.K. Vipparthi, S. Murala, S.K. Nagar, A.B. Gonde, Local gabor maximum edge position octal patterns for image retrieval, Neurocomputing 167 (2015) 336–345.

[65] S.K. Vipparthi, S.K. Nagar, Expert image retrieval system using directional local motif XoR patterns, Expert Syst. Appl. 41 (17) (2014) 8016–8026.

[66] S.K. Vipparthi, S.K. Nagar, Multi-joint histogram based modelling for image indexing and retrieval, Comput. Electr. Eng. 40 (8) (2014) 163–173.

[67] K. Yadav, A. Srivastava, A. Mittal, M.A. Ansari, Texture-based medical image retrieval in compressed domain using compressive sensing, Int. J. Bioinform. Res. Appl. 10 (2) (2014) 129–144.

[68] L. Yeffet, L. Wolf, Local trinary patterns for human action recognition, in: IEEE 12th International Conference on Computer Vision, ICCV 2009, 2011, pp. 492–497.

[69] G. Yue, D. Qionghai, W. Meng, Z. Naiyao, 3D model retrieval using weighted bipartite graph matching, Signal Process.: Image Commun. 26 (1) (2011) 39–47.

[70] C. Zenghai, Z. Hui, C. Zheru, F. Hong, Hierarchical local binary pattern for branch retinal vein occlusion recognition, in: ACCV Workshops, LNCS 9008, 1, pp. 687–697, 2014.

[71] B. Zhang, Y. Gao, S. Zhao, J. Liu, Local derivative pattern versus local binary pattern: face recognition with higher-order local pattern descriptor, IEEE Trans. Image Process. 19 (2) (2010) 533–544.

[72] L. Zhang, Z. Zhou, H. Li, Binary Gabor pattern: an efficient and robust descriptor for texture classification, in: 19th IEEE International Conference on Image Processing (ICIP), 2012, pp. 81–84.